Acta metall. mater. Vol. 41, No. 10, pp. 3007–3015, 1993
Printed in Great Britain.

0956-7151/93 $6.00 + 0.00

DETERMINATION OF THE INTERFACIAL TENSION BY ZERO CREEP EXPERIMENTS ON MULTILAYERS—I. THEORY

D. JOSELL† and F. SPAEPEN
Division of Applied Sciences, Harvard University, Cambridge, MA 02138, U.S.A.

(Received 18 December 1992)

Abstract—The zero creep load of a multilayered thin film is calculated for deformation by grain-boundary-diffusion-limited flow (Coble creep). A kinetic model is used to relate the zero creep load for uniaxial tension to the interfacial free energies and the grain dimensions.

1. INTRODUCTION

Interfacial free energies [1] or tensions, play an important role in nucleation, the coarsening of dispersions [2], grain growth [3], and intergranular brittle fracture [4]. The increasing use of composite materials has created a new impetus for their study [5, 6].

The standard method for an absolute measurement of an interfacial tension is based on the determination of the equilibrium angles at a triple point formed by the interface and two free surfaces, the tensions of which are known from zero creep experiments [7, 8]. Since the free surface tension can be strongly affected by adsorption and structural variations (reconstruction), the requirement that the free surfaces in the triple point and zero creep experiments be identical is a source of considerable uncertainty.

This paper describes how an interfacial tension can be measured *directly* in zero creep experiments on multilayered films with different interfacial areas. The need to reproduce free surfaces identical to those in earlier zero creep experiments, often under ultra-high vacuum, is eliminated. The free surfaces of the multilayers only need be the same in all creep runs, which can be accomplished by simple means and can be tested directly in zero creep experiments on pure films. In fact, the effect of the free surfaces can be made arbitrarily small by having a sufficiently large number of layers, and hence interfaces, in the multilayer.

The direct zero creep measurements of interfacial tensions are easier than those of free surface tensions in another way: since the number of interfaces in a multilayer can, in principle, be arbitrarily large, the zero creep load in the interfacial experiments is generally much higher, and hence easier to measure.

Continuous progress in the development of techniques for the deposition of multilayers makes it possible to create an increasing number of specific interfaces for these measurements.

2. EARLIER ZERO CREEP EXPERIMENTS

Udin *et al.* first used the zero creep technique to measure the free surface tension of copper [9], silver [10], and gold [11]. The theory [12] they developed for zero creep of a wire has been in use ever since [13–15]. Fisher and Dunn [16] extended it to zero creep of thin films. They took into account the constraints imposed on all four edges of the sample (fixed force or fixed displacement) and used a constitutive law relating stress and strain rate that is appropriate for homogeneous deformation (power law creep, Nabarro–Herring-type diffusive creep).

An extension of the Fisher–Dunn theory that takes account of the effects of grain boundaries was developed by Hondros [17]. He uses the same constitutive law, generalized to account for all three dimensions. The few zero creep experiments conducted on thin film samples have been analyzed with the Hondros theory [17–19].

Some zero creep experiments have been done on multi-component, single phase wires [20–24] and thin films [17, 19]. Most of that work dealt with the effect of a bulk alloying element on the surface tension. Some studied the changes in surface tension caused by surface adsorption from the vapor [19, 24].

3. THE "FLUX MODEL" OF ZERO CREEP

The Udin theory for the zero tensile creep load is *thermodynamic* in nature, in that it minimizes the free energy of the complete system of interfaces and load. This *minimization* is possible only if the strain in the tensile direction is the only independent variable. For Udin's cylindrical wire samples, this follows from the equilibrium shape of the cross-section (round, if isotropic) and the relation between length and radius

†Present address: NIST, Gaithersburg, MD 20899. U.S.A.

through the conservation of volume. In the Fisher–Dunn–Hondros theory for a thin film sample, the presence of three dimension variables necessitates the introduction of a constitutive flow law. They chose one that conserves volume and by which all volume elements of the grain deform identically.

In the zero creep experiments on multilayers described in the second paper, however, neither condition is satisfied. The grains in the individual layers do not have equilibrated cross-sections [25] and deform by grain-boundary-diffusion-governed flow (Coble creep), in which most of the volume elements in the grains do not deform at all. Therefore, it was necessary to develop a *kinetic* theory of zero creep, in which the fluxes of atoms are explicitly evaluated. This will be referred to as the "flux model" of zero creep.

The fluxes are driven by differences in the chemical potential on the grain faces which, in turn, depend on the applied load, the interfacial tensions, and the grain dimensions. Therefore, by setting the strain rate in the tensile direction, $\dot{\epsilon}_{\text{tensile}}$, equal to zero, the model can be used to determine the relationship between the zero creep load and the interfacial tensions.

A number of approximations needed to be made, since no analytical solution exists. First, the chemical potentials μ are defined at the center of each face as the average value over the entire face. The gradient of the chemical potential, $\nabla\mu$, used in calculating the fluxes, is approximated by using the difference in the values defined at the face centers, $\Delta\mu$, and the distance between the face centers l_{path}

$$\nabla\mu \approx \frac{\Delta\mu}{l_{\text{path}}}. \tag{1}$$

Second, all fluxes are assumed to follow the linear diffusion law

$$J(\text{No. atoms/sec} \cdot \text{area}) = -M_{\text{gb}} \nabla\mu \tag{2}$$

where M_{gb} is the atomic mobility on the grain boundary, assumed to be the same for all interfaces. If the mobility were assumed different for each type of boundary, they would appear in the final result in dimensionless combinations. Third, it is assumed that the layers are perfectly flat, which neglects the effect of grain boundary grooving. Of course, the grains in a thin film are no more orthorhombic than the grains in a wire specimen are cylindrical. However, for wires, the solution that accounts for the exact grain shape (in the absence of anisotropy) and Udin's cylindrical grain solution give zero creep loads that differ by less than 5%, [26] which is the typical experimental error. A similar result is anticipated here.

Consider a single grain from either layer, as illustrated in Fig. 1(c). Of the eight flux paths that include either the top or bottom face, and therefore contribute to $\dot{\epsilon}_{\text{tensile}}$, only two are unique. Adding these fluxes, weighted by their areas, A_i, gives the rate of atomic transfer that contributes to the strain in the tensile direction

$$\text{No. atoms/s} = -M_{\text{gb}} \sum_i A_i \frac{\Delta\mu_i}{l_i}. \tag{3}$$

Multiplying this atomic transfer rate by the atomic volume Ω, and dividing by the area TW of the upper or lower face gives the rate at which the length, L, of the grain changes

$$\dot{L} = -\frac{\Omega M_{\text{gb}}}{TW} \sum_i A_i \frac{\Delta\mu_i}{l_i}. \tag{4}$$

Normalization by the length L gives $\dot{\epsilon}_L$, the strain rate in the tensile direction

$$\dot{\epsilon}_L = -\frac{\Omega M_{\text{gb}}}{LTW} \sum_i A_i \frac{\Delta\mu_i}{l_i}. \tag{5}$$

The difference in chemical potential between the beginning and the end of the flux path has the form

$$\Delta\mu_i = -(\sigma_{\text{end}} - \sigma_{\text{beginning}})\Omega + \gamma_{\text{gb}} \Delta A_{\text{gb}}^{(i)} + \gamma_{\text{fs}} \Delta A_{\text{fs}}^{(i)} \tag{6}$$

where $\sigma_{\text{beginning}}$ and σ_{end} are the normal tractions on the interfaces at, respectively, the beginning and the end of the flux path. The other terms are changes in the total interfacial free energy of the system. Note that $\Delta\mu_i$ must be evaluated separately for each of the flux paths. The quantities $\Delta A_{\text{gb}}^{(i)}$, and $\Delta A_{\text{fs}}^{(i)}$ are defined as the changes in the grain boundary area, A_{gb}, and the free surface area, A_{fs}, when a single atom of volume Ω tranverses flux path i. This expression is appropriate regardless of the shape of the grain.

4. FLUX MODEL OF ZERO CREEP OF A MULTILAYER

The multilayer consists of a stack of identical bilayers. The zero creep load P_0 for a bilayer is evaluated using the flux method in the presence of different stress states, indicated by the second rank tensors $\sigma^{(1)}$ and $\sigma^{(2)}$, in layers 1 and 2 respectively. In the coordinates shown in Fig. 1(a), the stress tensors, by symmetry considerations, can be written in terms of the principal stresses $\sigma_i^{(j)}$ where the superscript represents the layer, either 1 or 2, and the subscript represents the component, or direction, and is between 1 and 3.

The six components of the two stress tensors are not independent. Demanding equal tractions at the interface between the layers yields

$$\sigma_1^{(1)} = \sigma_1^{(2)}, \tag{7}$$

and demanding that the internal stresses be consistent with the surface tractions yields

$$T_1\sigma_2^{(1)} + T_2\sigma_2^{(2)} = 0 \tag{8}$$

$$T_1\sigma_3^{(1)} + T_2\sigma_3^{(2)} = P/W_{\text{film}}. \tag{9}$$

Invoking the zero tractions on the front and back faces yields the additional constraint

$$\sigma_1^{(1)} = \sigma_1^{(2)} = 0. \tag{10}$$

The zero traction condition on the front and back surfaces can be invoked because the multilayer is thin in the normal direction. On the other hand, $\sigma_2^{(1)}$ and $\sigma_2^{(2)}$ change from zero to constant values over a distance from the film edges similar to the layer thickness. For the thin film case it is therefore legitimate to neglect the actual boundary conditions, or, equivalently, to assume that the surface tractions match the far-field stresses. The far-field stresses are calculated in what follows.

The strain tensors $\epsilon^{(1)}$ and $\epsilon^{(2)}$, also diagonal, are written in terms of their components $\epsilon_i^{(j)}$ using the same convention for superscript and subscript used for the stress tensor. The components of the strain rate tensors, $\dot{\epsilon}^{(1)}$ and $\dot{\epsilon}^{(2)}$, for small strains, are the time derivatives of the components of the strain tensors, $\dot{\epsilon}_i^{(j)}$. Because the layers are not free to move independently of each other, strain rates in the layers must be equal in the two in-plane directions

$$\dot{\epsilon}_3^{(1)} = \dot{\epsilon}_3^{(2)} \tag{11}$$

$$\dot{\epsilon}_2^{(1)} = \dot{\epsilon}_2^{(2)}. \tag{12}$$

Due to the constant-volume constraint in each layer, these two equalities imply equal strain rates in the third direction as well

$$\dot{\epsilon}_1^{(1)} = \dot{\epsilon}_1^{(2)}. \tag{13}$$

As seen on Fig. 1, the bilayer has total interfacial areas

$$A_{11} = n_{\mathrm{W}}^{(1)} T_1 L_{\mathrm{film}} - n_{\mathrm{L}}^{(1)} T_1 W_{\mathrm{film}} \tag{14}$$

$$A_{22} = n_{\mathrm{W}}^{(2)} T_2 L_{\mathrm{film}} - n_{\mathrm{L}}^{(2)} T_2 W_{\mathrm{film}} \tag{15}$$

$$A_{12} = 2 L_{\mathrm{film}} W_{\mathrm{film}} \tag{16}$$

where the subscript (ij) indicates an interface between materials i and j, $n_{\mathrm{W}}^{(i)}$ is the number of grain boundaries per width, W_{film}, in layer i, and $n_{\mathrm{L}}^{(i)}$ is the number of grain boundaries per unit length, L_{film}, in layer i. The factor of 2 (*not* 3) in (16) avoids double counting of the "free" surfaces in the multilayer as a whole. Because the bilayer is part of a multilayer, both "free" surfaces are considered identical to the internal interface between the layers, and all three are therefore assigned in interfacial tension γ_{12}. The interfaces within each layer are grain boundaries with average tensions γ_{11} and γ_{22}, for boundaries within layers 1 and 2 respectively.

In the derivation that follows, the two layers of the bilayer are treated separately. To do this, the interfacial tension γ_{12} is divided between the two resulting interfaces as $\beta\gamma_{12}$ for the surfaces of layer 1 and $(1-\beta)\gamma_{12}$ for the surfaces of layer 2, as illustrated in Fig. 1(b). Although it is possible to partition γ_{12}, [25] it is not necessary to do this here, since the final result turns out to be independent of the partitioning factor β.

To find the in-plane strain rates in layer 1, three unique fluxes are considered. For each there are a total of four equivalent paths, as labeled in Fig. 1(c). Each flux is modeled by a dimensional constraint imposed at constant grain volume: flux 1 is modeled by constant W_1 and grain volume $T_1 L_1 W_1$, flux 2 by constant T_1 and grain volume, and flux 3 by constant L_1 and grain volume.

For layer 1, now considered independently as in Fig. 1, the appropriate $\Delta\mu_i$ [equation (6)] for flux path$_i$ is

$$\Delta\mu_i = -(\sigma_{\mathrm{end}} - \sigma_{\mathrm{beginning}})\Omega + \gamma_{11}\Delta A_{11}^{(i)} + \beta\gamma_{12}\Delta A_{12}^{(i)}. \tag{17}$$

Dividing equation (14) by the number of grains in layer 1, $n_{\mathrm{L}}^{(1)} n_{\mathrm{W}}^{(1)}$, gives the grain boundary area associated with a single grain

$$A_{11} = T_1(L_1 + W_1). \tag{18}$$

Note that this is half the actual area to avoid double counting with neighboring grains. Similarly, dividing equation (16) by $n_{\mathrm{L}}^{(1)} n_{\mathrm{W}}^{(1)}$ gives the "free" surface associated with the grain

$$A_{12} = 2 L_1 W_1 \tag{19}$$

When an atom of volume Ω_1 migrates along path 1, while W_1 and the volume remain constant, the area changes are

$$\Delta A_{11}^{(1)} = -\frac{\Omega_1}{L_1} \tag{20}$$

$$\Delta A_{12}^{(1)} = 2\frac{\Omega_1}{T_1}. \tag{21}$$

Substitution of equations (20) and (21) in (17) yields

$$\Delta\mu_1 = -(\sigma_3^{(1)} - \sigma_1^{(1)})\Omega_1 - \gamma_{11}\frac{\Omega_1}{L_1} + 2\beta\gamma_{12}\frac{\Omega_1}{T_1} \tag{22}$$

which, because $\sigma_1^{(1)} = 0$ [equation (10)], simplifies to

$$\Delta\mu_1 = -\sigma_3^{(1)}\Omega_1 - \gamma_{11}\frac{\Omega_1}{L_1} + 2\beta\gamma_{12}\frac{\Omega_1}{T_1}. \tag{23}$$

When the same atom migrates along path 2, while T_1 and the volume remain constant, the area changes are

$$\Delta A_{11}^{(1)} = \Omega_1\left(\frac{1}{W_1} - \frac{1}{L_1}\right) \tag{24}$$

$$\Delta A_{12}^{(1)} = 0. \tag{25}$$

Substitution of equations (24) and (25) in (17) yields

$$\Delta\mu_2 = -(\sigma_3^{(1)} - \sigma_2^{(1)})\Omega_1 + \gamma_{11}\Omega_1\left(\frac{1}{W_1} - \frac{1}{L_1}\right). \tag{26}$$

When the same atom migrates along path 3, while L_1 and the volume remain constant, the area changes are

$$\Delta A_{11}^{(1)} = -\frac{\Omega_1}{W_1} \tag{27}$$

$$\Delta A_{12}^{(1)} = \frac{2\Omega_1}{T_1}. \tag{28}$$

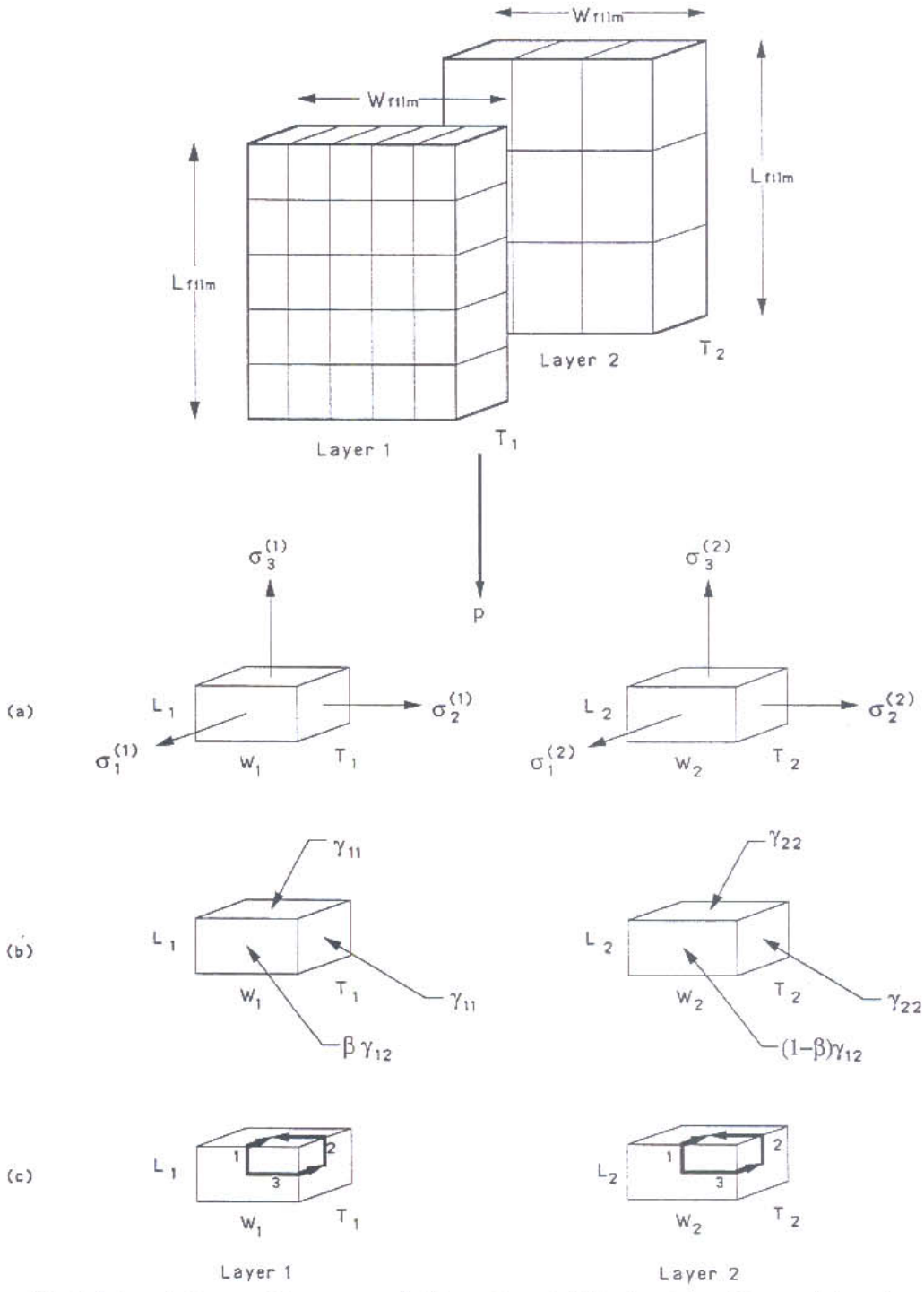

Fig. 1. Schematic diagram of the two parts of a bilayer. For an individual grain in each layer as indicated: (a) principal stresses; (b) assignment of interfacial and grain boundary free energies; (c) flux routes governing Coble creep.

Substitution of equations (27) and (28) in equation (17) yields

$$\Delta\mu_3 = -(\sigma_2^{(1)} - \sigma_1^{(1)})\Omega_1 - \gamma_{11}\frac{\Omega_1}{W_1} + \beta\gamma_{12}\frac{2\Omega_1}{T_1}. \quad (29)$$

Again, because $\sigma_1^{(1)} = 0$ [equation (10)] this simplifies to

$$\Delta\mu_3 = -\sigma_2^{(1)}\Omega_1 - \gamma_{11}\frac{\Omega_1}{W_1} + \beta\gamma_{12}\frac{2\Omega_1}{T_1}. \quad (30)$$

Finally, from Fig. 1(c), the path lengths l_i are

$$l_1 = \frac{(L_1 + T_1)}{2} \tag{31}$$

$$l_2 = \frac{(L_1 + W_2)}{2} \tag{32}$$

$$l_3 = \frac{(T_1 + W_1)}{2} \tag{33}$$

and the cross sections for the fluxes are

$$A_1 = 4W_1\delta_{gb} \tag{34}$$

$$A_2 = 4T_1\delta_{gb} \tag{35}$$

$$A_3 = 4L_1\delta_{gb} \tag{36}$$

where δ_{gb} is the grain boundary thickness. The factor of 4 accounts for the equivalent paths. Like M_{gb}, δ_{gb} is assumed to be the same on all surfaces.

Equation (5) becomes

$$\dot{\epsilon}_2^{(1)} = -\frac{\Omega_1 M_{gb}}{L_1 T_1 W_1} \sum_{i=1}^{2} A_1 \frac{\Delta\mu_i}{l_i}. \tag{37}$$

Substitution of equations (23), (26), (31), (32), (34), and (35) into equation (37) gives the expression for the strain rate in the tensile direction for layer 1

$$\dot{\epsilon}_3^{(1)} = \frac{-8\,\Omega_1^2 M_{gb}\delta_{gb}}{W_1 T_1 L_1} \cdot \left\{ \frac{W_1}{(L_1 + T_1)} \left(-\sigma_3^{(1)} - \gamma_{11}\frac{1}{L_1} + \beta\gamma_{12}\frac{2}{T_1} \right) + \frac{T_1}{(L_1 + W_1)} \left(-\sigma_3^{(1)} + \sigma_2^{(1)} + \gamma_{11}\left(\frac{1}{W_1} - \frac{1}{L_1} \right) \right) \right\}. \tag{38}$$

Figure 1(b) shows that the creep parameters for layers 1 map exactly onto those for layer 2 if β is replaced by $(1-\beta)$ and all superscripts and subscripts that indicate layer number are adjusted accordingly. Thus equation (38) can be modified to yield the corresponding strain rate in the tensile direction for layer 2

$$\dot{\epsilon}_3^{(2)} = \frac{-8\,\Omega_2^2 M_{gb}\delta_{gb}}{W_2 T_2 L_2} \cdot \left\{ \frac{W_2}{(L_2 + T_2)} \left(-\sigma_3^{(2)} - \gamma_{22}\frac{1}{L_2} + (1-\beta)\gamma_{12}\frac{2}{T_2} \right) + \frac{T_2}{(L_2 + W_2)} \left(-\sigma_3^{(2)} + \sigma_2^{(2)} + \gamma_{22}\left(\frac{1}{W_2} - \frac{1}{L_2} \right) \right) \right\}. \tag{39}$$

Using the relationships of equations (8) and (9) between the stresses in the different layers and the applied load P, this can be expressed in terms of the stresses in layer 1

$$\dot{\epsilon}_3^{(2)} = \frac{-8\,\Omega_2^2 M_{gb}\delta_{gb}}{W_2 T_2 L_2} \cdot \left\{ \frac{W_2}{(L_2 + T_2)} \left(-\frac{P}{T_2 W_{film}} + \frac{T_1}{T_2}\sigma_3^{(1)} - \frac{T_1}{T_2}\sigma_2^{(1)} + \gamma_{22}\left(\frac{1}{W_2} - \frac{1}{L_2} \right) \right) + \frac{T_2}{(L_2 + W_2)} \left(-\frac{P}{T_2 W_{film}} + \frac{T_1}{T_2}\sigma_3^{(1)} - \frac{T_1}{T_2}\sigma_2^{(1)} + \gamma_{22}\left(\frac{1}{W_2} - \frac{1}{L_2} \right) \right) \right\} \tag{40}$$

The strain rate in layer 1 in remaining in-plane direction is given by

$$\dot{\epsilon}_2^{(1)} = -\frac{\Omega_1 M_{gb}}{L_1 T_1 W_1} \left(A_3 \frac{\Delta\mu_3}{l_3} - A_2 \frac{\Delta\mu_2}{l_2} \right) \tag{41}$$

Substitution of equations (26), (30), (32), (33), (35) and (36) into equation (41) gives the expression for the strain rate of layer 1 in the nontensile, in-plane direction

$$\dot{\epsilon}_2^{(1)} = \frac{-8\,\Omega_1^2 M_{gb}\delta_{gb}}{W_1 T_1 L_1} \cdot \left\{ \frac{L_1}{(W_1 + T_1)} \left(-\sigma_2^{(1)} - \gamma_{11}\frac{1}{W_1} + \beta\gamma_{12}\frac{2}{T_1} \right) - \frac{T_1}{(L_1 + W_1)} \left(-\sigma_3^{(1)} + \sigma_2^{(1)} + \gamma_{11}\left(\frac{1}{W_1} - \frac{1}{L_1} \right) \right) \right\}. \tag{42}$$

The expression for $\dot{\epsilon}_2^{(2)}$, the strain rate in the same direction in layer 2, is derived through the same superscript and subscript changes that were used to derive $\dot{\epsilon}_3^{(2)}$ [equation (40)] from $\dot{\epsilon}_3^{(1)}$ [equation (38)]

$$\dot{\epsilon}_2^{(2)} = \frac{-8\,\Omega_2^2 M_{gb}\delta_{gb}}{W_2 T_2 L_2} \cdot \left\{ \frac{L_2}{(W_2 + T_2)} \left(-\sigma_2^{(2)} - \gamma_{22}\frac{1}{W_2} + (1-\beta)\gamma_{12}\frac{2}{T_2} \right) - \frac{T_2}{(L_2 + W_2)} \left(-\sigma_3^{(2)} + \sigma_2^{(2)} + \gamma_{22}\left(\frac{1}{W_2} - \frac{1}{L_2} \right) \right) \right\} \tag{43}$$

As was done for $\dot{\epsilon}_3^{(2)}$ in equation (40), the relationships of equations (8) and (9) between the stresses in the different layers and the applied load P can be used to express $\dot{\epsilon}_2^{(2)}$ in terms of the stresses in layer 1

$$\dot{\epsilon}_2^{(2)} = \frac{-8\,\Omega_2^2 M_{gb}\delta_{gb}}{W_2 T_2 L_2} \cdot \left\{ \frac{L_2}{(W_2 + T_2)} \left(\frac{T_1}{T_2}\sigma_2^{(1)} - \gamma_{22}\frac{1}{W_2} + (1-\beta)\gamma_{12}\frac{2}{T_2} \right) - \frac{T_2}{(L_2 + W_2)} \left(-\frac{P}{T_2 W_{film}} + \frac{T_1}{T_2}\sigma_3^{(1)} - \frac{T_1}{T_2}\sigma_2^{(1)} + \gamma_{22}\left(\frac{1}{W_2} - \frac{1}{L_2} \right) \right) \right\}. \tag{44}$$

Using equations (38), (40), (42), and (44), the compatibility requirements in the two in-plane directions [equations (11) and (12) respectively] can be solved to determine the unknown stresses $\sigma_2^{(1)}$ and $\sigma_3^{(1)}$

in terms of the applied load and grain dimensions. The strain rate of the film in the tensile direction can then be calculated by substituting the stresses into equation (38) for $\dot{\epsilon}_3^{(1)}$ or equation (40) for $\dot{\epsilon}_3^{(2)}$. The zero creep load P_0 is found by demanding

$$\dot{\epsilon}_3^{(1)} = 0 \tag{45}$$

in addition to the conditions of equations (11) and (12).

The grains in the layers are usually equiaxed in the plane. Therefore it can be assumed that $W_1 = L_1$ and $W_2 = L_2$, which simplifies the algebra considerably. The zero creep load then becomes

$$P_0 = W_{\text{film}}\left[2\gamma_{12} - \left(\frac{T_1}{W_1}\gamma_{11} + \frac{T_2}{W_2}\gamma_{22}\right)\right] \cdot \left\{1.0 + \frac{2B_1B_2(A_1T_2 + A_2T_1) + (T_2B_2A_1^2 + T_1B_1A_2^2)}{A_1A_2(T_2[(A_1 + 2B_1) + T_1(A_2 + 2B_2)]}\right\}^{-1} \tag{46}$$

where

$$A_i = \frac{\Omega_i^2}{T_iW_i(W_i + T_i)} \tag{47}$$

$$B_i = \frac{\Omega_i^2}{2W_i^3}. \tag{48}$$

When the aspect ratios, W_i/T_i, have the same value, x, in the two layers, P_0 has the particularly simple form

$$P_0 = 2W_{\text{film}}[2x^2\gamma_{12} - x(\gamma_{11} + \gamma_{22})]\frac{1}{2x^2 + x + 1}. \tag{49}$$

A naive mechanical estimate of the zero creep load is obtained by assuming that γ_{12} is a force per unit length that acts along the edge of the interface at the bottom of the film; per bilayer, that total edge length is $2W_{\text{film}}$. The "naive" value of the zero creep load is then $2W_{\text{film}}\gamma_{12}$. The present analysis, for square grains, shows that the correction factor from this value is

$$\Phi^{\text{square}}(x, y) \equiv \frac{P_0}{2W_{\text{film}}\gamma_{12}} = \frac{x(2x - y)}{1 + x + 2x^2} \tag{50}$$

where $y = (\gamma_{11} + \gamma_{22})/\gamma_{12}$. The quantities γ_{11}/γ_{12} and γ_{22}/γ_{12} can be experimentally obtained from measurements of triple point angles in the creep specimens themselves [27]. A representative plot of Φ^s, for a given value of y, can be seen in Fig. 3. For small aspect ratios, x, the zero creep load is compressive, as indicated by the negative value of Φ^s.

If the two elements are assumed to have different mobilities M_i, still independent of the type of interface, equation (46) still applies, but equations (47) and (48) are replaced by

$$A_i = \frac{M_i\Omega_i^2}{T_iW_i(W_i + T_i)} \tag{51}$$

$$B_i = \frac{M_i\Omega_i^2}{2W_i^3}. \tag{52}$$

If one of the elements has a higher mobility on the grain boundaries (i.e. $M_1 \gg M_2$) equation (46) can again be simiplified, using equations (51) and (52), without the assumption of equal aspect ratios in the two layers, to equation (50), but with $x = x_2$ and $y = (\gamma_{11}x_2/x_1 + \gamma_{22})/\gamma_{12}$, where $x_1 = W_1/T_1$ and $x_2 = W_2/T_2$. Thus, the aspect ratio, x_1, of the layer containing the more mobile species appears only in the effective grain boundary tension for bilayers composed of elements with considerably different mobilities.

Application of the flux method to a single layer thin film yields a formula for the nondimensionalized zero creep load that is identical to (50) if $\gamma_{12} = \gamma_{\text{fs}}$, the free surface tension, $y = \gamma_{\text{gb}}/\gamma_{\text{fs}}$, and $x = W/T$.

5. FLUX MODEL OF ZERO CREEP OF A THIN FILM COMPOSED OF HEXAGONAL GRAINS

In order to estimate the magnitude of the geometrical uncertainties in the previous analysis, creep in a film with hexagonal grains has also been analyzed. The results are similar to those for the square grains.

Figure 2 shows the sample geometry and grain shape. Of the 12 flux paths that contribute to the $\dot{\epsilon}_{\text{tensile}}$ only two are unique by symmetry considerations. The six side faces within the layer are grain boundaries with an interfacial tension γ_{gb}. They are assigned an area

$$A_{\text{gb}} = T(B + 2C) \tag{53}$$

to avoid double counting. The front and back faces are free surfaces with an interfacial tension γ_{fs} and area

$$A_{\text{fs}} = \sqrt{3}(C^2 + 2BC) \tag{54}$$

To determine the strain rate $\dot{\epsilon}_{\text{tensile}}$, the net atomic flow from (3) is multiplied by the atomic volume Ω and divided by the area of the surface to which the atoms are migrating, $TC\sqrt{3}$, and by the average length of the grain, $B + C/2$

$$\dot{\epsilon}_{\text{tensile}} = -\frac{\Omega M_{\text{gb}}}{TC\sqrt{3}(B + C/2)}\sum_i A_i\frac{\Delta\mu_i}{l_i}. \tag{55}$$

Here, and in the following calculations of $\Delta A_{\text{gb}}^{(i)}$ and $\Delta A_{\text{fs}}^{(i)}$ used in $\Delta\mu_i$ (6), it is assumed that the migrating volume Ω is deposited uniformly over the entire top surface, with $\Omega/2$ on each side. This maintains a space filling structure and keeps the grain dimensions unambiguous. Because the resulting extension is in the tensile direction, the applied stress, not its normal component, will appear in the expressions for $\Delta\mu_i$ [26].

To determine the incremental areas $\Delta A_{\text{gb}}^{(i)}$ and $\Delta A_{\text{fs}}^{(i)}$ in equation (6), flux 1 is modeled by leaving T and the grain volume constant. Flux 2 is modeled by leaving C and the grain volume constant.

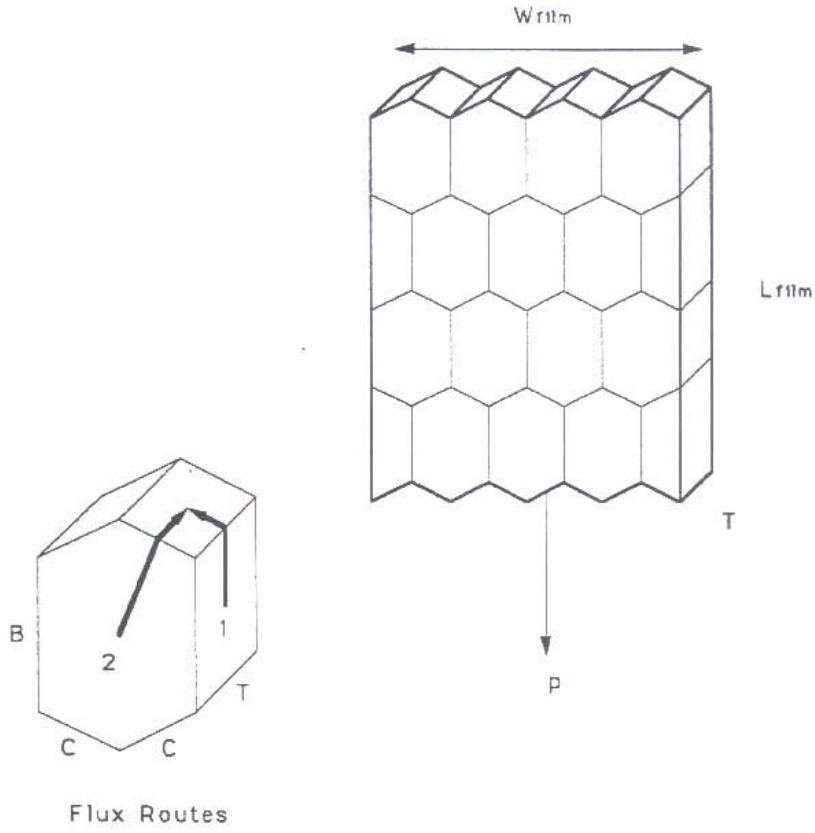

Fig. 2. Schematic diagram of a thin film composed of hexagonal columnar grains. The flux routes governing Coble creep are indicated on an individual grain.

From equations (53) and (54), and the constraints for flux route 1, the migration of a single atom of volume Ω along route 1 is seen to result in the area changes

$$\Delta A_{gb}^{(1)} = \frac{\Omega}{\sqrt{3}}\left(\frac{1}{C} - \frac{1}{B}\right) \tag{56}$$

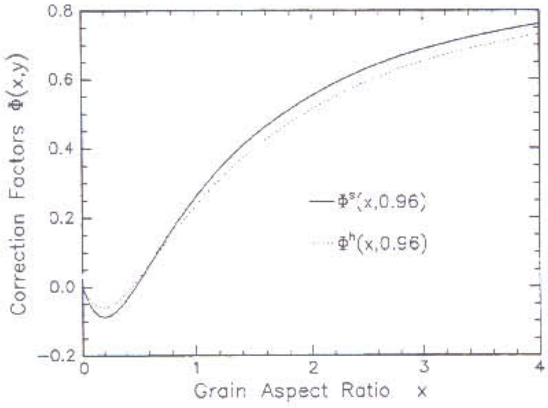

Fig. 3. Correction factor, Φ, to the "naive" zero creep load, $2W_{film}\gamma_{12}$, as a function of the aspect ratio, x, of an equiaxed grain for a given value (0.96) of the ratio of the grain boundary to interfacial free energies. Solid line: square grain; dotted line: hexagonal grain of equal volume.

and

$$\Delta A_{fs}^{(1)} = 0. \tag{57}$$

The migration of the same atom along flux route 2 is seen to result in

$$\Delta A_{gb}^{(2)} = \frac{-\sqrt{3}\Omega}{(2B + C)} \tag{58}$$

and

$$\Delta A_{fs}^{(2)} = \frac{2\Omega}{T}. \tag{59}$$

Using (6), the difference in the chemical potential for the two flux routes can now be written

$$\Delta\mu_1 = -\sigma\Omega + \gamma_{gb}\frac{\Omega}{\sqrt{3}}\left(\frac{1}{C} - \frac{1}{B}\right) \tag{60}$$

$$\Delta\mu_2 = -\sigma\Omega - \gamma_{gb}\frac{\sqrt{3}\Omega}{(2B + C)} + \gamma_{fs}\frac{2\Omega}{T}. \tag{61}$$

Finally, from Fig. 2, the path lengths l_i are

$$l_1 = \frac{(B + C)}{2} \tag{62}$$

$$l_2 = \tfrac{1}{2}(\sqrt{B^2 + C^2 + BC} + T) \tag{63}$$

and the cross section of flux, is

$$A_1 = 4T\delta_{gb} \tag{64}$$

$$A_2 = 8C\delta_{gb} \tag{65}$$

where δ_{gb} and M_{gb} are defined the same way as in the case of the cubic grains. The factors of 4 and 8 in the expressions for A_i arise from the equivalent paths.

Substitution of (60) through (65) into (55) yields

$$\dot{\epsilon}_{tensile} = \frac{-16\Omega^2 M_{gb}\delta_{gb}}{(2B+C)TC\sqrt{3}} \times \left\{ \frac{T}{B+C}\left(-\sigma + \gamma_{gb}\frac{1}{\sqrt{3}}\left(\frac{1}{C}-\frac{1}{B}\right)\right) + \frac{2C}{\sqrt{B^2+C^2+BC}+T} \times \left(-\sigma - \gamma_{gb}\frac{\sqrt{3}}{2B+C} + \gamma_{fs}\frac{2}{T}\right)\right\}. \tag{66}$$

As with the square case, the equiaxed morphology of the grains allows the substitution $B = C$, which yields

$$\dot{\epsilon}_{tensile} = \frac{16\,\Omega^2 M_{gb}\delta_{gb}}{3C^2T\sqrt{3}} \times \left\{ -\sigma\left(\frac{T}{2C} + \frac{2C}{\sqrt{3}C+T}\right) + \frac{2C}{\sqrt{3}C+T}\left(-\gamma_{gb}\frac{1}{\sqrt{3}C} + \gamma_{fs}\frac{2}{T}\right)\right\}. \tag{67}$$

Setting $\dot{\epsilon}_{tensile} = 0$ gives the zero creep stress

$$\sigma_0 = \frac{4C^2}{T^2+4C^2+TC\sqrt{3}}\left(\gamma_{fs}\frac{2}{T} - \gamma_{gb}\frac{1}{\sqrt{3}C}\right) \tag{68}$$

and, using $P_0 = TW_{film}\sigma_0$ for the thin film geometry

$$P_0 = 2W_{film}\gamma_{fs}\frac{2(C/T)^2}{1+4(C/T)^2+\sqrt{3}C/T} \times \left(2 - \frac{\gamma_{gb}/\gamma_{fs}}{\sqrt{3}C/T}\right). \tag{69}$$

Substitution of the nondimensional length variable $x_h \equiv C/T$ and the nondimensional free energy variable $y \equiv \gamma_{gb}/\gamma_{fs}$ yields the correction factor, similar to equation (50)

$$\Phi^{hex}(x_h, y) \equiv \frac{P_0}{2\gamma_{fs}W_{film}} = \frac{4x_h\left(x_h - \dfrac{y}{2\sqrt{3}}\right)}{4x_h^2 + \sqrt{3}x_h + 1}. \tag{70}$$

To compare $\Phi^{square}(x_s, y)$ with equation (70), the grain volume TW^2 for the cubic case is equated with that for the hexagonal case, $(3\sqrt{3})/2\,TC^2$. Or

$$C = W\sqrt{\frac{2}{3\sqrt{3}}} \tag{71}$$

so that

$$x_{hexagon} = \frac{C}{T} = \frac{W}{T}\sqrt{\frac{2}{3\sqrt{3}}} = x_{square}\sqrt{\frac{2}{3\sqrt{3}}} \approx 0.620x_{square}.$$

Substituting this into equation (70) gives

$$\Phi^{hex}_{film}(x_h \approx 0.62x_s, y) \equiv \frac{1.538x_s^2 - 0.716x_s y}{1.538x_s^2 + 1.074x_s + 1} \tag{72}$$

which can now be compared directly to equation (50) for the single layer with cubic grains.

The correction functions $\Phi^{hex}(0.62x_s, y)$ and $\Phi^{square}(x_s, y)$ are plotted as functions of x_s in Fig. 3 for a representative value of γ_{gb}/γ_{fs}. It is evident that both functions have a similar dependence on the grain aspect ratio. Thus the flux model seems insensitive to the exact shape of the grains, as long as they are equiaxed. This makes it possible to analyze the results for samples with a wide variety of two-dimensional equiaxed grain shapes with a single model.

Acknowledgements—This work has been supported by the Office of Naval Research under contract number N00014-91-J-1281. D. Josell gratefully acknowledges the generous support of the Fannie and John Hertz Foundation.

REFERENCES

1. J. W. Cahn, in *Interfacial Segregation* (edited by W. C. Johnson and J. M. Blakely), pp. 3–23. ASM, Metals Park, Ohio (1979).
2. G. W. Greenwood, *Acta metall.* **4**, 243 (1956).
3. W. W. Mullins, *Acta Metall.* **6**, 414 (1958).
4. J. R. Rice and J.-S. Wang, *Mater. Sci. Engng* **A107**, 23 (1989).
5. E. R. Fuller Jr, E. P. Butler and W. C. Carter, *Toughening Mechanisms in Quasi-Brittle Materials* (edited by S. P. Shah), p. 385. Kluwer Academic, Amsterdam (1991).
6. T. W. Coyle, E. R. Fuller Jr and P. Swanson, *Ceram. Engng Sci. Proc.* **8**, 630 (1987).
7. J. E. Hilliard, M. Cohen and B. L. Averbach, *Acta metall.* **8**, 26 (1960).
8. C. A. Handwerker, J. M. Dynys, R. M. Cannon and R. L. Coble, *J. Am. Ceram. Soc.* **73**, 1371 (1990).
9. H. Udin, A. J. Shaler and J. Wulff, *Metall. Trans. A.I.M.E.*, p. 186, Feb. (1949).
10. E. R. Funk, H. Udin and J. Wulff, *Trans A.I.M.E., J. Metals*, p. 1206, Dec. (1951).
11. F. H. Buttner, H. Udin and J. Wulff, *Trans. A.I.M.E., J. Metals*, p. 1209, Dec. (1951).
12. H. Udin, *Trans. A.I.M.E.* **189**, 63 (1951).
13. A. T. Price, H. A. Holl and A. P. Greenough, *Acta metall.* **20**, 617 (1972).
14. L. F. Bryant, R. Speiser and J. P. Hirth, *Trans. A.I.M.E.* **242**, 1145 (1968).
15. T. Heumann and J. Johannisson, *Acta metall.* **20**, 617 (1972).
16. J. C. Fisher and C. G. Dunn, in *Imperfections in Nearly Perfect Crystal* (edited by W. Shockley), p. 317. Wiley, New York (1952).
17. E. D. Hondros, *Proc. R. Soc.* **A286**, 479 (1965).

18. G. A. Jablonski and A. Sacco Jr, *J. Mater. Res.* **6**, 744 (1991).
19. E. D. Hondros and L. E. H. Stuart, *Phil. Mag.* **17**, 711 (1968).
20. M. C. Inman, D. McLean and H. R. Tipler, *Proc. R. Soc.* **A273**, 438 (1963).
21. B. C. Allen, *Trans. A.I.M.E.* **236**, 903 (1966).
22. L. E. Murr, R. J. Horylev and G. I. Wong, *Surf. Sci.* **26**, 184 (1971).
23. L. E. Murr, G. I. Wong and R. J. Horylev, *Acta metall.* **21**, 595 (1973).
24. H. Jones and G. M. Leak, *Acta metall.* **14**, 21 (1966).
25. F. Spaepen, in *Surface Layers: Structure–Property Relations* (edited by M. A. J. Somas and E. Mittemeijer), IOP, London (1993).
26. D. Jossell, Ph.D. thesis, Harvard Univ. (1992).
27. D. Josell and F. Spaepen, *Acta metall. mater.* **41**, 3017 (1993).